ACS OMEGA

Open Access

http://pubs.acs.org/journal/acsodf

Article

Structural Diversity and Dimensionality of Three Cu(II)-dpds-$C_5O_5^{2-}$ Coordination Polymers Controlled by the Coordination Sphere of Cu(II) Centers and the Coordination Modes of $C_5O_5^{2-}$ (dpds = 4,4′-Dipyridyldisulfide)

Chih-Chieh Wang,* Pei-Juan Liao, Yu-Chen Chung, Chi-Yang Shin, Yi-Chen Wu, Gene-Hsiang Lee, Su-Ying Chien, Bo-Hao Chen, and Yu-Chun Chuang*

Cite This: *ACS Omega* 2024, 9, 40920−40931

Read Online

ACCESS | Metrics & More | Article Recommendations | Supporting Information

ABSTRACT: Three supramolecular architectures, $[Cu_2(dpds)_2(C_5O_5)_2(H_2O)_4]\cdot 3H_2O$ (**1**), $[Cu(dpds)(C_5O_5)]\cdot 3H_2O$ (**2**), and $[Cu_2(dpds)_2(C_5O_5)_2]\cdot 9H_2O\cdot C_2H_5OH$ (**3**) (dpds = 4,4′-dipyridyldisulfide and $C_5O_5^{2-}$ (croconate) = dianion of 4,5-dihydroxycyclopent-4-ene-1,2,3-trione), have been synthesized and structurally characterized. Compound **1** contains two crystallographically independent Cu(II) ions, which are both distorted octahedral geometry with elongation along the croconate- and H_2O-bound axial positions and bonded with two N atoms of two dpds, two O atoms of one $C_5O_5^{2-}$, and two H_2O molecules. Two crystallographically independent dpds ligands, both adopting the bis-monodentate bridging mode, connect two Cu(II) ions to form a one-dimensional zigzag chain-like coordination polymer. In **2** and **3**, there are two and three crystallographically independent Cu(II) ions, respectively, which are all distorted octahedral geometries with elongation along the croconate-bound axial positions six-coordinated and bonded with two N atoms of two dpds ligands in cis- or/and trans-forms and four O atoms of two $C_5O_5^{2-}$ ligands. The dpds ligands in **2** and **3** all adopt the bis-monodentate bridging mode, and the $C_5O_5^{2-}$ ligands act as bridging ligands with bridging bis-bidentate through three $C_5O_5^{2-}$ oxygen atoms in **2** and bridging bis-bidentate through four adjacent $C_5O_5^{2-}$ oxygen atoms in **3**, respectively, linking the Cu(II) ions to generate a two-dimensional layered and a three-dimensional metal−organic framework, respectively. The structural diversity and dimensionality observed in **1**−**3** may be attributed to the cis- or/and trans-coordination sphere of Cu(II) centers with two dpds ligands and the coordination modes of croconate ligands. Thermal stability and in situ temperature-dependent structural variations of **1**−**3** have been verified by thermogravimetric analysis and powder X-ray diffraction measurements. Compounds **1** and **3** both exhibit water vapor capture behaviors with hysteresis isotherms.

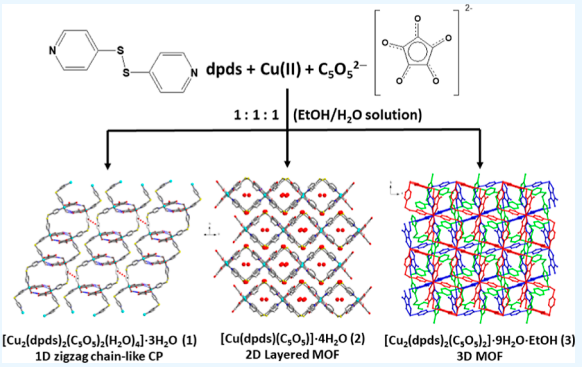

INTRODUCTION

The construction of three-dimensional (3D) supramolecular structures built up via the assembly of metal−organic frameworks (MOFs)[1,2] or CPs[1] has been the subject of significant interest over recent decades not only due to the variety of their structural topologies and 3D supramolecular architectures but also due to their potential applications in various fields.[3−10] For the construction of suitable MOFs or CPs, the choice of organic ligands or metal ions and the reactivity of the linkers play an important role.[11] However, many other factors, e.g., the use of auxiliary ligands, additive, template, and reaction conditions, such as temperature, solvent, and pH, can affect the structural diversity and topology of the MOFs.[12−16] Thus, their controlled synthesis and structural prediction are still worth further investigation. Multitropic ligands with various coordination modes have been widely used in the construction of CPs or MOFs and are now at the core of supramolecular coordination chemistry.[17] Recently, porous 3D MOFs have been examined for their water capture properties, and they were found to be highly promising materials.[18−20] Three distinct pathways, including chemisorption on open metal sites, physisorption in the form of layers or clusters, or capillary condensation, can be found during the water adsorption in MOFs.[18,20] However, water capture behaviors applied on 3D supramolecular networks assembled via 0D metal complexes, one-dimensional (1D) CPs, or two-dimensional (2D) MOFs are seldom, and only few

Received: July 3, 2024
Revised: September 5, 2024
Accepted: September 11, 2024
Published: September 18, 2024

Scheme 1. Coordination Modes of Croconate Ligands: (a) Monodentate (I), (b) Bidentate Chelate (II), (c) μ-1,2-Monodentate (III), (d) μ-1,3-Monodentate (IV), (e) μ-1,2-Bidentate-1-μ-oxo (V), (f) μ-1,2-Bidentate-3-monodentate (VI), (g) μ-1,2-Bidentate-3-monodentate (VII), (h) μ-1,2,3,4-bis-bidentate (VIII), (i) μ-1,2,3-bis-bidentate (IX), (j) μ3-1,2-bidentate-2-μ-oxo-3-monodentate (X), (k) μ3-1,2-bidentate-3-μ-oxo (XI), (l) μ3-1-Monodentate-2,3,4,5-bis-bidentate (XII), (m) μ3-1,2,3-bis-bidentate-4,5-bidentate (XIII), (n) μ3-1,2,3-bis-bidentate-1-μ-oxo (XIV), and (o) μ4-1,2,3,4-bis-bidentate-1,4-μ-oxo (XV)

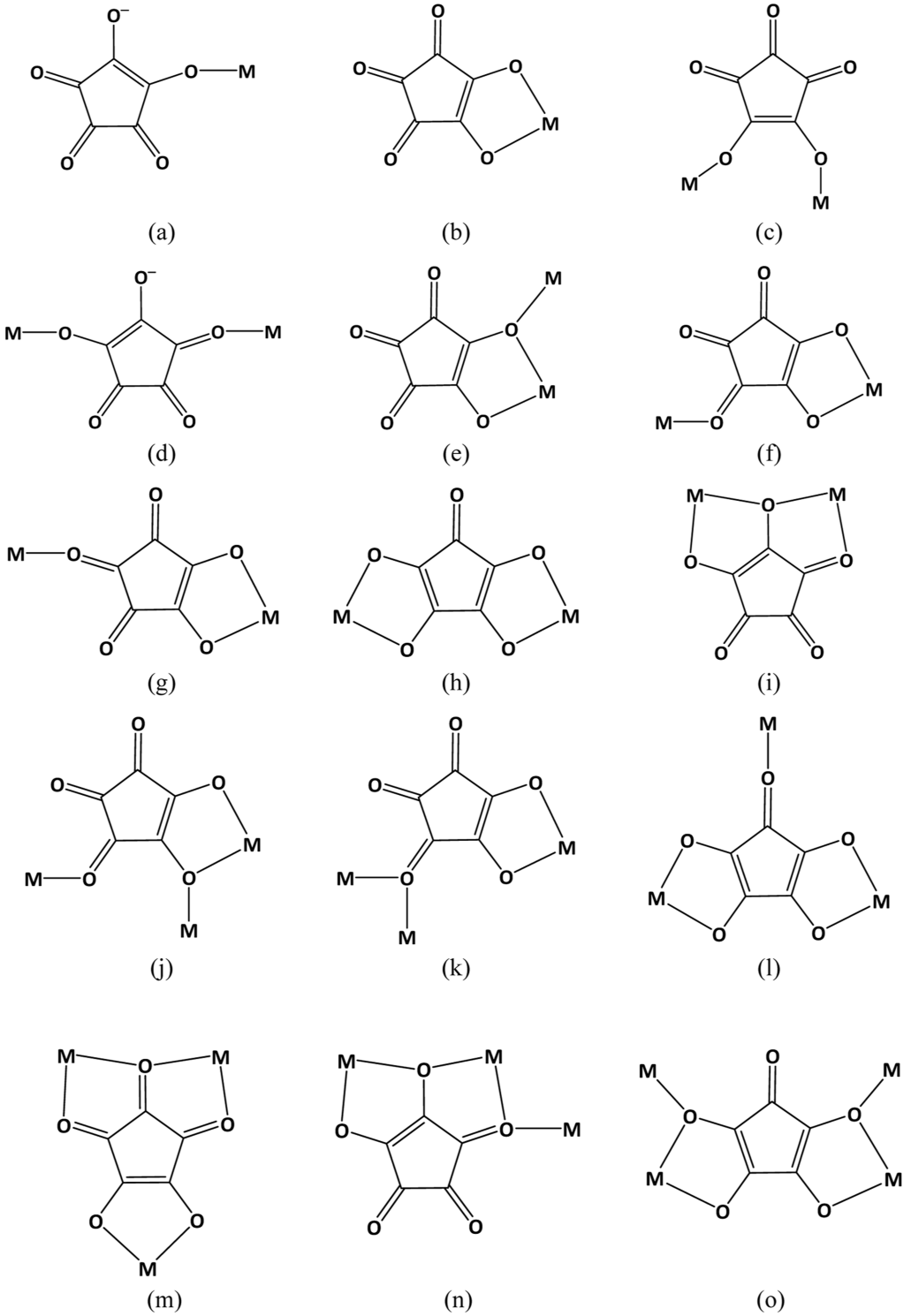

cases have been examined.[21−23] Metal complexes of croconate ($C_5O_5^{2-}$, dianion of 4,5-dihydroxycyclo-pent-4-1,2,3-trione) associated with pyridyl-based coligands and the bonding characteristics of croconate with transition metal ions and lanthanide ions have been widely investigated.[24−49] This cyclic oxocarbon dianion ligand has been widely used as a polyfunctional linker not only acting as a ligand coordinate to the metal ions with various coordination modes[50] (Scheme

https://doi.org/10.1021/acsomega.4c06176
ACS Omega 2024, 9, 40920−40931

1) as monodentate (I), bidentate chelate (II), μ-1,2-monodentate (III), μ-1,3-monodentate (IV), μ-1,2-bidentate-1-μ-oxo (V), μ-1,2-bidentate-3-monodentate (VI), μ-1,2-bidentate-3-monodentate (VII), μ-1,2,3,4-bis-bidentate (VIII), μ-1,2,3-bis-bidentate (IX), μ3-1,2-bidentate-2-μ-oxo-3-monodentate (X), μ3-1,2-bidentate-3-μ-oxo (XI), μ3-1-monodentate-2,3,4,5-bis-bidentate (XII), μ3-1,2,3-bis-bidentate-4,5-bidentate (XIII), μ3-1,2,3-bis-bidentate-1-μ-oxo (XIV), and μ4-1,2,3,4-bis-bidentate-1,4-μ-oxo (XV), on the construction of versatile 0D metal complexes, 1D polymeric chains, and 2D or 3D MOFs but also as a hydrogen bonding acceptor and/or a $\pi-\pi$ constructor on the construction of extended supramolecular architectures. In our previous study, we have employed croconate associated with *N*,*N*′-dipyridyl-based rod-like spacer ligands to create mixed-ligand 2D MOFs, e.g., $[Cd_2(C_5O_5)_2(4,4'\text{-bpy})(H_2O)]_\infty$ (4,4′-bpy = 4,4′-bipyridine),[47] $[M(C_5O_5)(dpe)]$ (M = Mn, Fe, Co, and Cd; dpe = 1,2-bis(4-pyridyl)ethane),[40,48] and $[M_2(C_5O_5)_2(bpe)(H_2O)]\cdot nH_2O$ (M = Ni, Zn, n = 1; M = Cd, n = 2; and bpe = 1,2-bis(-4-pyridyl)ethylene),[44,49] respectively, where two types of bridging coordination modes of croconate ligands have been used on the extension of their structural dimensions. Two kinds of 3D supramolecular architectures are created by assembly of interlocked 2D layered MOFs[44,47] and 2D bilayered MOFs,[40,44,48,49] respectively, via the bridged M(II) ions with related *N*,*N*′-dipyridyl-based ligands and croconate, and their thermal stability and thermal structural variations have been studied by thermogravimetric analysis (TGA) and in situ powder X-ray diffraction (PXRD) measurements.[40,44,47−49] However, no related structural characterization of mixed-ligand Cu(II)−croconate CPs or MOFs is found and is worthy of further study. In order to explore the effects of coordination modes of croconate and coordination environments of Cu(II) ions on the structural diversity and dimensionality of mixed-ligand metal−croconate CPs or MOFs, we employ another flexible *N*,*N*′-dipyridyl-based ligand, 4,4′-dipyridyldisulfide (dpds), for the first time, to obtain three Cu(II) supramolecular architectures, a 1D chain of $[Cu_2(dpds)_2(C_5O_5)_2(H_2O)_4]\cdot 3H_2O$ (**1**), a 2D layer framework of $[Cu(dpds)(C_5O_5)]\cdot 3H_2O$ (**2**), and a 3D network of $[Cu_2(dpds)_2(C_5O_5)_2]\cdot 9H_2O\cdot EtOH$ (**3**). The structural characterization and thermal stability as well as the water adsorption/desorption isotherms of compounds **1**−**3** will be studied and discussed in details.

EXPERIMENTAL SECTION

General Procedures and Physical Measurements. All solvents for syntheses were of analytical grade and were used without further purification. All chemical reagents were obtained from commercial suppliers and were used without further purification. Infrared (IR) spectra were recorded with samples in the form of KBr pellets on a PerkinElmer 1600 spectrometer. The elementary analyses were performed by using a PerkinElmer 2400 elemental analyzer. TGA measurements were conducted on a PerkinElmer 7 Series/UNIX TGA7 analyzer. The gas [N_2 (77 K) and CO_2 (194 K)] and water vapor (298 K) adsorption experiments were performed using BELSORP-max volumetric adsorption equipment from BEL, in Osaka, Japan. The adsorbent samples (∼100−150 mg), which has been prepared at 200 °C for **1**, 200 °C for **2**, and 150 °C for **3**, respectively, and 10^{-2} Pa for about 24 h prior to measurement of the isotherm, were then placed into the sample cell (∼1.8 cm^3). The change of pressure was monitored, and the degree of adsorption was determined by the decrease of pressure at equilibrium state.

Synthesis of $[Cu_2(dpds)_2(C_5O_5)_2(H_2O)_4]\cdot 3H_2O$ (1), $[Cu(dpds)(C_5O_5)]\cdot 3H_2O$ (2), and $[Cu_2(dpds)_2(C_5O_5)_2]\cdot 9H_2O\cdot EtOH$ (3). An EtOH/H_2O solution (3 mL) of $Na_2C_5O_5$ (1.9 mg, 0.01 mmol) was added to an EtOH/H_2O solution (6 mL) of $CuCl_2\cdot 2H_2O$ (1.7 mg, 0.01 mmol) and dpds (2.2 mg, 0.01 mmol) at room temperature, which gave a pale-yellow solution. The resulting solution was allowed to stand for several days, and then crystallizing of pale-green columnar-like crystals of **1**, green block-like crystals of **2**, and dark-green needle-like crystals of **3** in the yields of 43% (2.1 mg), 5% (0.2 mg), and 30% (1.6 mg), respectively, in the EtOH/H_2O (v/v = 1:1) solution (solution 1) based on $CuCl_2\cdot 2H_2O$ was performed. In order to obtain a single product of **1**, **2**, and **3**, respectively, and increase the yields of **2**, we try to change the reaction conditions, including reaction temperatures, molar ratios of reactants, and volume ratios of ethanol and H_2O solutions. Unfortunately, no matter what reaction conditions we have tried, the mixtures, at least two products among **1**, **2**, and **3**, are produced. However, the yields of **2** were successfully increased as the solution volume ratio is changed to EtOH/H_2O (v/v) = 1:4 (solution 2), with the yields of 29% (1.4 mg), 44% (2.1 mg), and 19% (1.0 mg) for **1**, **2**, and **3**, respectively, based on $CuCl_2\cdot 2H_2O$. For the isolation of compounds **1**, **2**, and **3**, due to the crystal shapes and colors of **1**, **2**, and **3** being obviously different, they can be differentiated under the microscopy. So, we work hard to isolate the pure crystals of the single product from the mixtures of **1**, **2**, and **3** by mechanical separation with picking crystals under the microscopy. The yields of crystals **1**−**3** were collected by both repeated synthesis protocol and increasing the synthetic amounts of reactants from 0.01 to 0.1 mmol (solution 1 plus solution 2) for consequent characterization of PXRD, TGA, and sorption experiments. Anal. Calcd for $C_{30}H_{30}Cu_2N_4O_{17}S_4$ (**1**): C, 37.00; N, 5.75; H, 3.10. Found (solution 1): C, 36.99; N, 5.89; H, 2.70 and Found (solution 2): C, 37.12; N, 5.61; H, 2.66. Anal. Calcd for $C_{15}H_{14}Cu_1N_2O_8S_2$ (**2**): C, 37.69; N, 5.86; H, 2.95. Found (solution 1): C, 38.10; N, 5.49; H, 2.61 and Found (solution 2): C, 38.23; N, 5.75; H, 2.26. Anal. Calcd for $C_{32}H_{40}Cu_2N_4O_{20}S_4$ (**3**): C, 36.39; N, 5.30; H, 2.65. Found (solution 1): C, 36.43; N, 5.72; H, 2.75 and Found (solution 2): C, 36.13; N, 5.04; H, 2.21. Selected IR data of **1** (cm^{-1}, KBr pellet): 3106 (m), 3091 (m), 3065 (m), 1717 (m), 1591 (s), 1523 (vs), 1488 (vs), 1411 (s), 1318 (m), 1214, (m), 1056 (m), 1022 (m), 818 (m), 714 (m) cm^{-1}. Selected IR data of **2** (cm^{-1}, KBr pellet): 3466 (w), 3094 (w), 3066 (w), 1719 (m), 1672 (m), 1593 (s), 1476 (vs), 1415 (s), 1318 (m), 1216 (m), 1103 (m), 1061 (m), 1030 (m), 814 (m), 720 (m) cm^{-1}. Selected IR data of **3** (cm^{-1}, KBr pellet): 3092 (m), 3036 (m), 1716 (w), 1592 (s), 1521 (vs), 1486 (vs), 1416 (s), 1318 (m), 1214 (m), 1101 (w), 1057 (m), 1022 (w), 818 (m), 717 (m) cm^{-1}. The IR spectra of **1**−**3** (Figures S6−S8) from solution 1 and solution 2, respectively, are provided in the Supporting Information.

Crystallographic Data Collection and Refinement. The single-crystal X-ray diffraction data of compounds **1**, **2**, and **3** at 150 K and **3** at 295 K, respectively, were individually collected on a Bruker D8 Venture diffractometer equipped with a Mo-target (Kα = 0.71073 Å) microfocus X-ray generator and a PHOTON-II CMOS detector. The temperature was adjusted with a nitrogen flow (Oxford Cryosystems, 800 series). The cell refinement and data integration were

https://doi.org/10.1021/acsomega.4c06176
ACS Omega 2024, 9, 40920−40931

Scheme 2. Schematic Synthetic Representation of Compounds 1−3

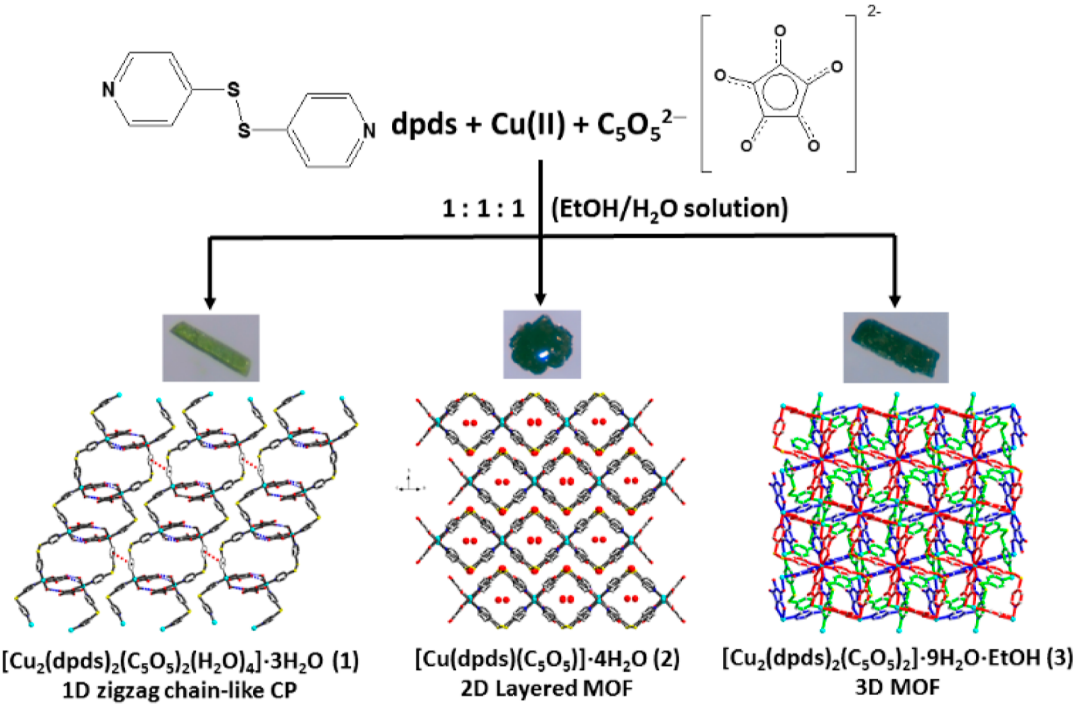

carried out by the Bruker SAINT[51] software package using a narrow-frame algorithm and were collected for absorption effects using the Multi-Scan method (SADABS[52]). The crystal structure was solved by the SHELXT program, and the structure refinements were performed by the SHELXTL[53] Software. For compounds **1**−**3**, all hydrogen atoms of dpds ligands were generated geometrically, and hydrogen atoms of the coordinated, solvated water and ethanol molecules were located in the difference Fourier map with the corresponding positions and isotropic displacement parameters being refined. The final full-matrix, least-squares refinement on F^2 was applied for all observed reflections $[I > 2\sigma(I)]$. All calculations were performed using APEX4[54] software. Crystallographic data and details of data collections and structure refinements of **1**, **2**, and **3** at 150 and 295 K are listed in Table S1. CCDC2246199, CCDC2246200, CCDC2246201, and CCDC2246202 for **1**, **2**, and **3** at 150 K and **3** at 295 K, respectively, contain the supplementary crystallographic data for this paper. These data can be obtained free of charge at www.ccdc.cam.ac.uk/conts/retrieving.html [or from the Cambridge Crystallographic Data Centre, 12, Union Road, Cambridge CB2 1EZ, UK; fax: (Internet.)+44-1223/336-033; Email:deposit@ccdc.cam.ac.uk.

Temperature-Dependent PXRD. High-resolution PXRD measurements were performed at TPS 19A in the National Synchrotron Radiation Research Center, Taiwan. An incident X-ray photon energy of 16 keV (λ = 0.77489 Å) was employed for **1** and **2**, and 20 keV (λ = 0.61992 Å) was employed for **3**. The PXRD patterns were recorded by a 1D position-sensitive detector, MYTHEN 18K. All samples were packed into 0.3 mm borosilicate glass capillaries and were fast rotated at 500 rpm during data collection. All the geometry and sample position offset corrections were calibrated using the NIST standard material, LaB_6(660c), using the GSAS-II suite[55] and GSASII scriptable module.[56] A hot air gas blower was placed 2 mm under the sample with a ramp rate of 0.2 °C/s for high-temperature experiments. To improve the statistical robustness of the data, diffraction data was collected at each temperature for five seconds and merged over ten frames.

RESULTS AND DISCUSSION

Synthesis and IR Spectroscopy of Compounds 1−3. Compounds **1**−**3** are synthesized in a one-pot reaction, and their synthetic representations are shown in Scheme 2. It is important to note that the yields of **1**, **2**, and **3** can be modified by changing the relative EtOH/H_2O (v/v) ratio in the mixing solution. If the mixing solution of EtOH/H_2O (v/v) ratio is 1/1 (solution 1), the yields of **1**, **2**, and **3** are 43%, 5%, and 30%, respectively. When the mixing solution of EtOH/H_2O (v/v) ratio is changed to 1/4 (solution 2), the yields of **1**, **2**, and **3** are changed to 29%, 44%, and 19%, respectively. This result suggests that with decreasing ethanol content in the solvent, the yield of **2** increases. Due to obviously different colors and shapes of crystals **1**, **2**, and **3** in the solution (as shown in Scheme 2), compounds **1**, **2**, and **3** were isolated and collected by mechanically separating crystals carefully from the reaction mixture. All of the resulting products are stable in air at ambient temperature, and the synthetic reproducibility is very nice. The IR features related to dpds and $C_5O_5^{2-}$ ligands for **1**−**3** are almost identical throughout the region from 500 to 3200 cm^{-1}. Strong absorptions occurring in the range 1500−1700 cm^{-1} are characteristic of the salts of $C_5O_5^{2-}$ ligands and can be assigned to vibrational modes representing mixtures of C−O and C- stretching motions.[57] The medium-strength absorptions at 1716, 1719, and 1717 cm^{-1} for **1**, **2**, and **3**, respectively, are assigned to the uncoordinated carbonyl C═O groups of the $C_5O_5^{2-}$ ligand. The broad bands for **1**, **2**, and **3** in the region 3000−3200 cm^{-1} can be assigned to the ν(O−H) stretching vibrations of the water molecules.

Structural Description of $[Cu_2(dpds)_2(C_5O_5)_2(H_2O)_4]\cdot 3H_2O$ (1). Compound **1** is iso-structural with $[Co_2(dpds)_2(C_5O_5)_2(H_2O)_4]\cdot 3H_2O$.[46] Due to Jahn−Teller distortion of d^9 Cu(II) ions, two crystallographically

https://doi.org/10.1021/acsomega.4c06176
ACS Omega 2024, 9, 40920−40931

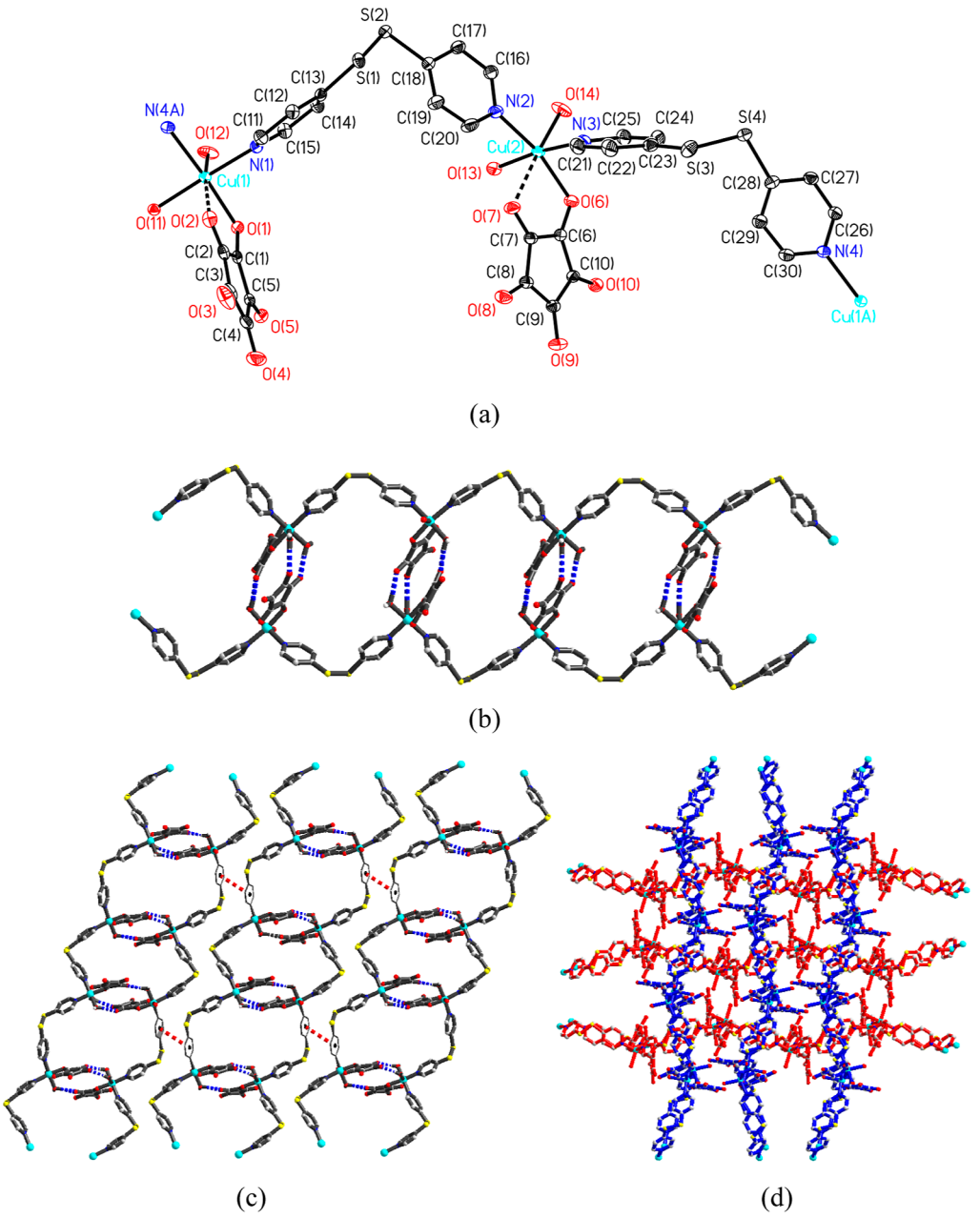

Figure 1. (a) Coordination spheres of two Cu(II) ions in **1** (ORTEP drawing, 50% thermal ellipsoids). Hydrogen atoms and guest H_2O molecules are omitted. (b) Hydrogen-bonded 1D ladder-like polymeric bichains. (c) 2D layered framework assembled by $\pi-\pi$ stacking interaction between 1D hydrogen-bonded ladder-like polymeric bichains. (d) 3D supramolecular network assembled by 2D layered frameworks arranged orderly in a combined ABAB··· parallel and interpenetrating manner.

independent Cu(II) ions are both elongated, distorted octahedral bonded to two dpds N atoms and one water and one croconate O atoms in the equatorial plane (shown in Figure 1a), and a second croconate oxygen atom and the other water molecule in the axial positions with Cu(1)−O(12) 2.259(8), Cu(1)−O(2) 2.496(9), Cu(2)−O(14) 2.179(6), and Cu(2)−O(7) 2.486(6), respectively (Table S2 provided in the Supporting Information). In **1**, two crystallographically independent dpds ligands both adopt a bis-monodentate bridging mode, linking the Cu(II) ions to generate a 1D zigzag chain-like coordination polymer. The Cu(1)···Cu(2) separations via bridges of dpds ligands are 11.616(1) and 10.779(1) Å. Meanwhile, two polymeric chains are mutually interlinked to generate a 1D hydrogen-bonded ladder-like polymeric bichain framework (shown in Figure 1b, green dashed lines) via three interchain O−H···O hydrogen bonding interactions between coordinated H_2O molecules and uncoordinated O atoms of asymmetrical bidentate chelate $C_5O_5^{2-}$ ligands (Scheme 1b). The Cu(1)···Cu(2) separation via hydrogen-bonded interchain linkage is 8.270(2) Å. Furthermore, adjacent bichains are assembled via interchain $\pi-\pi$ stacking interaction (shown in Figure 1c, purple dashed lines) between two pyridyl rings of neighboring dpds ligands with a ring centroid distance of 4.532 Å (Table S4 provided in the Supporting Information) to extend to a composite hydrogen-bonded plus $\pi-\pi$ stacked 2D layered frameworks (Figure 1c). Adjacent 2D layers are then arranged orderly in a combined parallel ABAB··· allay and mutually interpenetrating manner to

https://doi.org/10.1021/acsomega.4c06176
ACS Omega 2024, 9, 40920−40931

construct its 3D supramolecular networks (shown in Figure 1d) via two interlayer O−H···O hydrogen bonds between the uncoordinated O atoms of $C_5O_5^{2-}$ and coordinated H_2O molecules of neighboring layers. It is interesting to note that three guest H_2O molecules all behave as two hydrogen-bonded donors and one hydrogen-bonded acceptor and are mutually linked via hydrogen bonds to generate a $(H_2O)_3$ trimer. The synergistic interactions occur via the hydrogen bonds between the $(H_2O)_3$ trimer and uncoordinated O atoms of $C_5O_5^{2-}$ and coordinated H_2O molecules, providing an extra-stabilization energy to keep the aggregation of $(H_2O)_3$ water trimers in the 3D supramolecular network. Related parameters for O−H···O hydrogen bonds are listed in Table S3 (provided in the Supporting Information).

Structural Description of $[Cu(dpds)(C_5O_5)]\cdot 3H_2O$ (2). The asymmetric unit (ASU) of **2** composes of two Cu(II) ions, one dpds, one $C_5O_5^{2-}$, and three solvated guest H_2O molecules, in which two crystallographically independent Cu(II) ions [Cu(1) and Cu(2)] are both $\{CuN_2O_4\}$ six-coordinate-coordinated to four O atoms of two $C_5O_5^{2-}$ ligands and two N atoms of two dpds ligands in a cis-form for Cu(1) ions (located at the 2-fold axis) and a trans-form for Cu(2) ions (located at the inversion center), respectively (as shown in Figure 2a). Due to Jahn−Teller distortion of d^9 Cu(II) ions, both of two Cu(II) ions have a nearly octahedral surrounding, showing elongation along the croconate-bound axial positions with Cu(1)−O(2) 2.461(4) and Cu(2)−O(2) 2.267(3), respectively (Table S5 provided in the Supporting Information). In **2**, the dpds ligand adopts a bis-monodentate bridging mode, connecting Cu(1) and Cu(2) ions to form a 1D zigzag polymeric chain. The Cu(1)···Cu(2) separation via the dpds bridge is 10.684(6) Å. Adjacent chains are arranged in an alternate ABAB··· fashion and then interlinked via the bridges of Cu(II) ions and $C_5O_5^{2-}$ ligand adopting an asymmetrical μ-1,2,3-bis-bidentate coordination mode (Scheme 1i) to form a 2D layered MOF (Figure 2b), generating 1D rectangle-grid-like open channels (Figure 2c, side view). The separation of Cu(1)···Cu(2) via the $C_5O_5^{2-}$ bridge is 4.646(6) Å. Adjacent 2D layered MOFs are then arranged orderly in an ABAB··· manner to construct its 3D supramolecular network (Figure 2d). It is noteworthy that the synergistic interactions occur between three seriously disordered guest H_2O molecules and 2D MOFs via the O−H···O hydrogen bonds providing extra-stabilization energy, holding the guest H_2O molecules intercalated into the vacant spaces in the microporous 3D supramolecular architecture (Figure 2d). Related parameters for the −H···O hydrogen bonds are listed in Table S6.

Structural Description of $[Cu_2(dpds)_2(C_5O_5)_2]\cdot 9H_2O\cdot$ EtOH (3). The ASU of **3** is composed of three Cu(II) ions, two dpds ligands, two $C_5O_5^{2-}$ ligands, nine solvated H_2O, and one ethanol molecules, in which three crystallographically independent Cu(II) ions are all CuN_2O_4 six-coordinate-coordinated to two N atoms of two dpds ligands and four O atoms of two $C_5O_5^{2-}$ ligands in trans-form for Cu(1) and Cu(2) ions (both located at inversion centers) and cis-form for Cu(3) ions, respectively (shown in Figure 3a). Due to Jahn−Teller distortion of d^9 Cu(II) ions, all three Cu(II) ions have a distorted octahedral surrounding, showing elongation along the croconate-bound axial positions with Cu(1)−O(2) 2.475(2), Cu(2)−O(7) 2.510(2), Cu(3)−O(9) 2.485(2), and Cu(3)−O(4) 2.517(3), respectively (Table S7 provided in the Supporting Information). In **3**, both the dpds and $C_5O_5^{2-}$ act as bridging ligands with a bis-monodentate and an

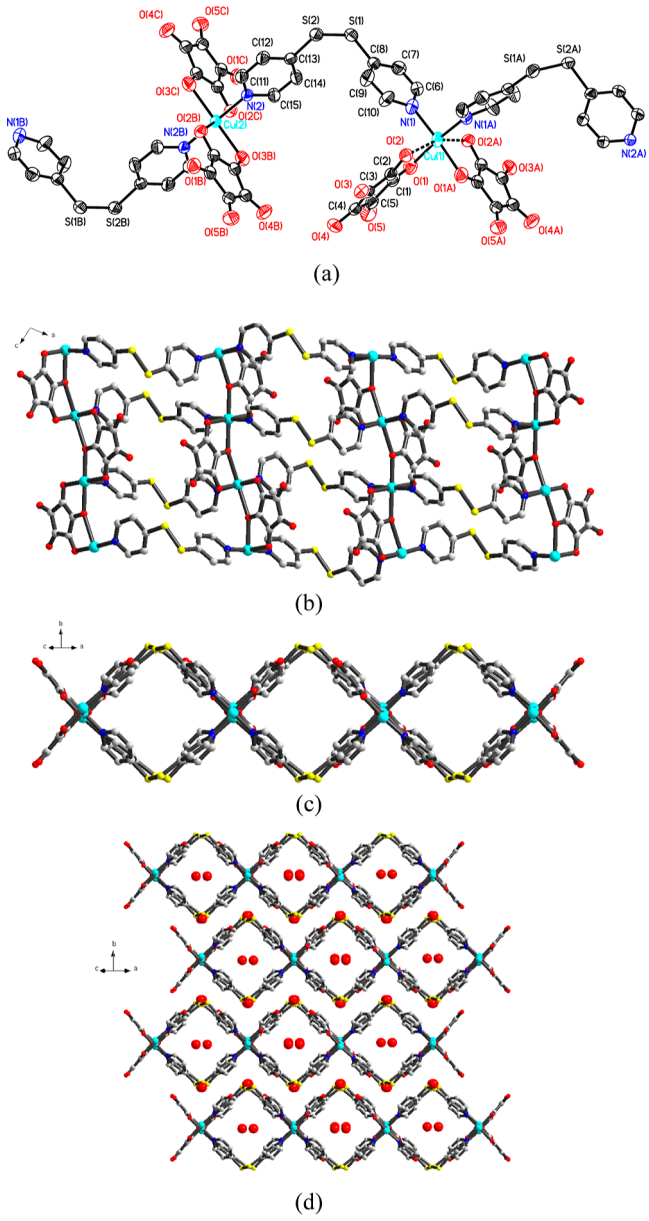

Figure 2. (a) Coordination spheres of two Cu(II) ions in **2** (ORTEP drawing, 50% thermal ellipsoids). Hydrogen atoms and solvated H_2O molecules are omitted. (b) 2D layered MOF viewing along the *b* axis and (c) side view along the ⟨1 0 1⟩ direction generating square-grid-like channels. (d) 3D supramolecular architecture assembled by 2D MOFs in an alternate ABAB··· manner.

unusual asymmetrical μ-1,2,3,4-bis-bidentate coordination modes (Scheme 1h), respectively, connecting three Cu(II) ions to form a 1D framework (shown in Figure 3b) with a $[Cu_3(C_5O_5)_2(dpds)]$ rectangle-grid metallocycle as the basic building unit. The Cu(1)···Cu(2) distance via one dpds bridge is 9.982(3) Å, and the Cu(1)···Cu(3) and Cu(2)···Cu(3) distances via two crystallographically independent $C_5O_5^{2-}$ bridges are 6.835(3) and 6.872(3) Å, respectively. Furthermore, adjacent 1D frameworks are arranged orderly in a parallel and alternate ABAB··· manners (the red and blue ones shown in Figure 3c) and mutually interlinked via the connectivity of cis-coordination Cu(3) ions and the other dpds ligands (the green ones shown in Figure 3d) to generate a microporous 3D MOF (Figure 3c,d). The Cu(3)···Cu(3)

https://doi.org/10.1021/acsomega.4c06176
ACS Omega 2024, 9, 40920−40931

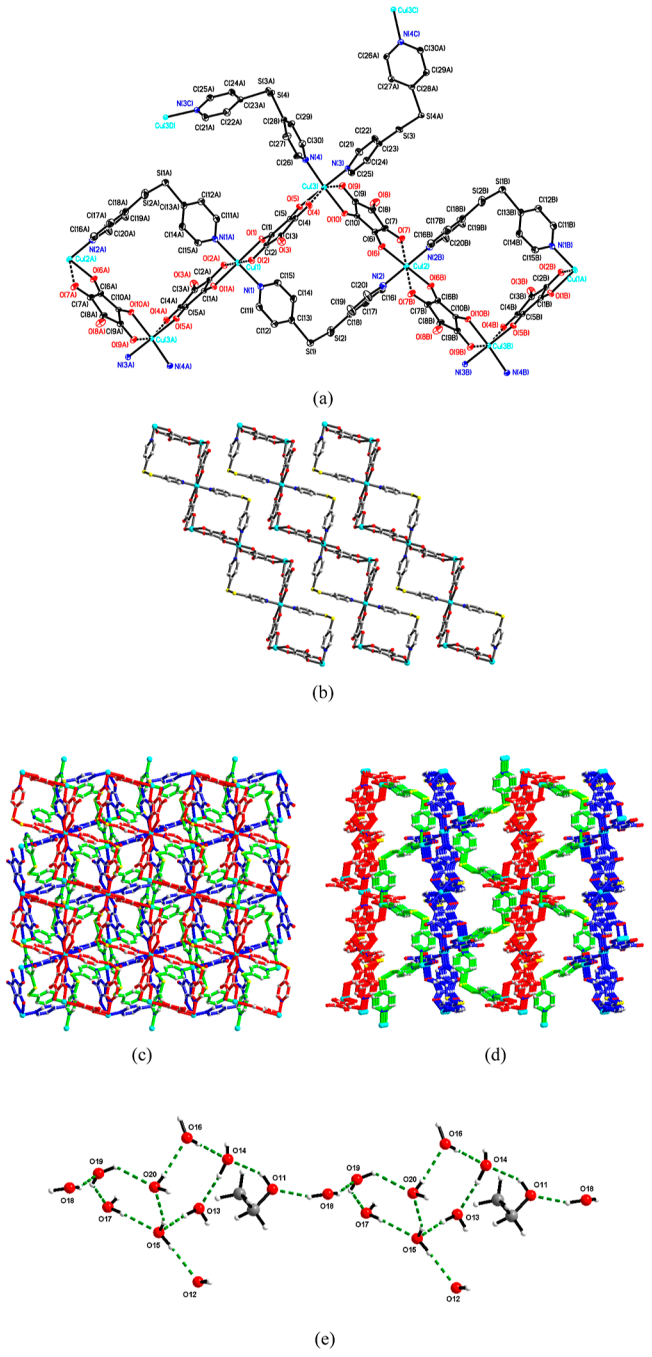

Figure 3. (a) Coordination spheres of three Cu(II) ions in **3** (ORTEP drawing, 50% thermal ellipsoids). Hydrogen atoms and guest H_2O and C_2H_5OH molecules are omitted. (b) 1D frameworks with $[Cu_3(C_5O_5)_2(dpds)]$ metallocycle square-grid as the basic building unit. The 3D MOF viewing along (c) *a* axis and (d) *c* axis. (e) 1D hydrogen-bonded chains assembled by 9 water and 1 EtOH guest molecules with an unusual $(H_2O)_7$ water cluster showing edge-shared five-membered and four-membered rings.

distance via the other dpd bridge is 11.413(3) Å. It is noteworthy that all the guest molecules, including one C_2H_5OH and nine H_2O molecules, are mutually interlinked via O−H···O hydrogen bonds to generate a 1D hydrogen-bonded chain, containing an unusual $(H_2O)_7$ water cluster showing edge-shared five-membered and four-membered rings (shown in Figure 3e). Meanwhile, the synergistic interactions occur between the solvent molecules and 3D MOF via the O−H···O hydrogen bonding interactions between the solvent molecules and O atoms of $C_5O_5^{2-}$ ligands, providing extra-stabilization energy holding the aggregation of 1D hydrogen-bonded chains intercalated into the channels of the microporous 3D MOF. Related parameters of O−H···O hydrogen bonds are listed in Table S8.

Thermal Stability and Structural Variation of 1−3. The thermal stability associated with temperature-dependent structural variation of **1**−**3** was studied and carried out by TGA and in situ temperature-dependent PXRD measurements. TGA (Figure S1(a), provided in the Supporting Information) reveals that **1** was thermally stable up to 67.7 °C and then underwent a two-step weight loss of total 12.6% in the temperature ranges of 67.7−94.6 and 145.6−182.4 °C, respectively, approximately equal to the weight losses of seven water molecules (calcd. 12.9%) with three solvated and four coordinated water molecules and then thermally stable up to 250.0 °C. The first-step weight losses of 9.0% approximately correspond to the losses of five water molecules (calcd. 9.2%), equal to the removal of three solvated and two coordinated water molecules with two longer $Cu-O_{water}$ bonds of 2.179(6) and 2.259(8) Å, and the second-step weight losses of 3.6% approximately correspond to the losses of the other two coordinated water molecules (calcd. 3.7%). The IR spectrum of **1** (shown in Figure S6(c)) after being heated at 190 °C shows that all the peaks for dpds and $C_5O_5^{2-}$ ligands are retained, except the broad peaks around 3000−3400 cm^{-1} at room temperature because the O−H bonds of coordinated water molecules disappeared, indicating the formation of a dehydrated form of **1**, which is in accordance with the result of TGA. On further heating, sample **1** decomposed. TGA (Figure S2(a)) reveals that **2** underwent a one-step weight loss in the approximate temperature range of 30.2−108.6 °C, with the weight loss of 11.8%, approximately equal to the losses of three guest water molecules (calcd. 11.4%) and then thermally stable up to 236.3 °C. Similar to **1**, the IR spectrum of **2** (shown in Figure S7(c)) after being heated at 150 °C also shows that all the peaks for dpds and $C_5O_5^{2-}$ ligands are retained, except the broad peaks around 3000−3400 cm^{-1} at room temperature because the O−H bonds of coordinated water molecules disappeared, indicating the formation of a dehydrated form of **2**, which is also in accordance with the result of TGA. On further heating, sample **2** decomposed. TGA (Figure S3(a)) reveals that **3** underwent a one-step weight loss in the approximate temperature range of 32.9−138.2 °C, with the weight loss of 14.1%, approximately equal to the losses of 8 solvated water molecules (calcd. 14.7%) and then thermally stable up to 240.8 °C. Similar to **1** and **2**, the IR spectrum of **3** (shown in Figure S8(c)) after being heated at 150 °C also shows that all the peaks for dpds and $C_5O_5^{2-}$ ligands are retained, except the broad peaks around 3000−3400 cm^{-1} at room temperature because the O−H bonds of coordinated water and EtOH molecules disappeared, indicating the formation of a dehydrated form of **3**, which is also in accordance with the result of TGA. On further heating, sample **3** decomposed. The inconsistency between the experimental weight loss (14.1%) and calculated weight loss (19.7% of 9 H_2O and 1 C_2H_5OH, based on structural determination at 150 K) may be deduced to the partial losses of solvent molecules in **3** at RT. In order to prove the deduction, the crystal structure of **3** was redetermined at 295 K by the single-crystal X-ray diffraction method. The structural characteristics of **3** at 295 K are almost the same as those at 150 K. The only difference is

https://doi.org/10.1021/acsomega.4c06176
ACS Omega 2024, 9, 40920−40931

the numbers and types of solvent molecules existed in the vacant spaces, where 9 H_2O and 1 EtOH molecules are found at 150 K, but only 8 water molecules are found at 295 K. The calculated weight loss of 14.7% for 8 H_2O molecules at 295 K is very close to the weight loss of 14.1% observed from the TGA.

In situ high-resolution PXRD experiments of **1**−**3** were performed and analyzed to investigate the temperature-dependent structural variations during the thermal dehydration procedures (Figures S1(b), S2(b), and S3(b), provided in the Supporting Information for **1**, **2**, and **3**, respectively). The crystalline structure of complex **2** remains stable up to 90 °C, as evidenced by the close match between the powder pattern at room temperature and the simulated pattern. However, an evident phase transformation occurs above 110 °C, corresponding to the dehydration of the samples. This phase change was further investigated using the Le Bail cell refinement (Table S9, provided in the Supporting Information), which revealed significant structural alterations during dehydration. Due to the serious disorder behaviors of the organic ligand dpds and packing solvents, obtaining an accurate structural model from high-temperature diffraction data is challenging, even at 150 K. Despite this, the Le Bail cell refinement provided critical insights into the cell parameters and structural transformations. The unit cell volume is highly correlated to the chemical formula and Z, with a simple approximation being that each element, including hydrogen atoms, occupies ∼12.5 $Å^3$. For example, the low-temperature structure, with a volume of 3746 $Å^3$, is consistent with the formula $C_{15}H_{10}CuN_2O_8S_2$, considering the C-centered lattice and $Z = 4$, which corresponds to approximately 38 elements. Thermal expansion and dehydration significantly impact the unit cell. Notably, the unit cell shrank along the *a*-axis by about 2.16 Å during the dehydration process, indicating that the pores of the square-grid-like 1D channels closed. This is further evidenced by the overall unit cell volume reduction of 726 $Å^3$ at high temperatures (150 °C), which correlates with the loss of 2−3 packing water molecules, as supported by TGA results. The dehydration also causes the interlayer distance along the *b*-axis in the 2D layered MOF to decrease after the removal of water molecules packed between the square-grid-like channels. Additionally, the loss of water molecules within these channels leads to distortion along the *a*-axis and a reduction in the beta angle from 99.7 to 97.1°.

At room temperature, the powder pattern of **1** closely matches the simulated pattern. A phase transition occurs between 110 and 130 °C, corresponding to the dehydration of the samples. The cell parameters of the dehydrated form of **1** were determined using the Le Bail method and are provided in Table S9 (available in the Supporting Information). A significant volume reduction in the lattice is observed after dehydration at temperatures exceeding 130 °C. Similarly, at room temperature, the powder diffraction patterns of **3** closely resemble the simulated pattern, with only minor discrepancies due to solvent disorder and differences in occupancy ratios. However, as the temperature rises above 90 °C, the diffraction pattern changes, and the crystallinity decreases. Between 110 and 175 °C, the samples undergo desolvation, with solvent molecules being removed from the crystal structure. The structural changes observed in the temperature-dependent PXRD measurements are consistent with the TGA results. Based on similar estimates from **2**′, the volumes of **1**′ and **3**′ are approximately 3341 and 3295 $Å^3$, respectively, which correspond to the dehydrated formula $[Cu_2(dpds)_2(C_5O_5)_2]$, approximately matching the expected count of 65 elements.

Water Vapor Adsorption/Desorption Isotherms of 1−3. The N_2 gas isotherms of **1**−**3** at 77 K all revealed a typical type-II adsorption profile (Figure S4a−c) with low N_2 gas uptake, suggesting only surface adsorption. The CO_2 gas adsorption isotherms of dehydrated **1**−**3** at 195 K all revealed very low CO_2 gas uptakes (see Figure S5 provided in the Supporting Information). To understand the water adsorption capability and the interactions between water molecules and the flexible frameworks, we performed water vapor measurements on pretreated dehydrated samples of **1**, **2**, and **3** at ambient conditions. For dehydrated **1**, the water adsorption isotherm (Figure 4a) shows a type-II adsorption isotherm[58,59] with a steady increase of adsorbed water vapor at 0 < relative P/P_0 < 1.00, with a maximum value of 91.6 $cm^3\ g^{-1}$ at relative P/P_0 equal to 0.99, roughly equal to 3.98 water molecules per ASU. The result reveals that the dehydrated **1** may readsorb approximately 4 water molecules. It is worth noting that the desorption curve did not follow the adsorption curve any longer and exhibited a significant hysteresis loop with a value of 41.1 $cm^3\ g^{-1}$ (roughly equal to 1.8 water molecules per ASU) at lower relative P/P_0 equal to 0.04, which may indicate that the Cu(II) center of the dehydrated samples provides the vacant sites for the bond reformation with water molecules. **1** exhibits hysteretic adsorption behavior to water molecules not only because it has easily accessible hydrogen-bonded interaction sites from the O atoms of $C_5O_5^{2-}$ but also by reason for the unsaturated Cu(II) sites to generate the strong adsorbate−adsorbent interaction. For water vapor adsorption of dehydrated **2**, the water adsorption isotherm (Figure 4b) shows a type-I adsorption isotherm[58,59] characterized by a water uptake at low pressure with a sudden increase of adsorbed water vapor at 0.00 < relative P/P_0 < 0.05, with a value of 20.66 $cm^3\ g^{-1}$ at relative P/P_0 equal to 0.04, roughly equal to 0.61 water molecules per ASU; after that, a steady increase of adsorbed water vapor at 0.04 < relative P/P_0 < 1.02, with a maximum value of 72.3 $cm^3\ g^{-1}$ at relative P/P_0 equal to 1.00, roughly equal to 2.11 water molecules per ASU, indicated that the dehydrated **2** can readsorb approximately 2.0 guest water molecules. The desorption curve also did not follow the adsorption curve but exhibited a small hysteresis loop with a value of 25.35 $cm^3\ g^{-1}$ (roughly equal to 0.75 water molecules per ASU) at lower relative P/P_0 equal to 0.03. For dehydrated **3**, the water adsorption isotherm (Figure 4c) also shows type-II adsorption isotherm[51,52] with a steady increase of adsorbed water vapor at 0 < relative P/P_0 < 0.86, with a maximum value of 74.0 $cm^3\ g^{-1}$ at relative P/P_0 equal to 0.86, roughly equal to 3.5 water molecules, and then an abrupt increase of adsorbed water vapor at 0.86 < relative P/P_0 < 1.00, with a maximum value of 110.85 $cm^3\ g^{-1}$ at relative P/P_0 equal to 1.00, roughly equal to 5.2 water molecules, indicated that the dehydrated **3** can readsorb about 5 guest water molecules in **3**. Similar to **1**, the desorption curve also did not follow the adsorption curve any longer, which also exhibited a large hysteresis loop with a value of 59.3 $cm^3\ g^{-1}$ (roughly equal to 2.8 water molecules) at lower relative P/P_0 equal to 0.04. **3** exhibits hysteretic adsorption behavior to water molecules, which may be attributed to easily accessible hydrogen-bonded interaction sites from the O atoms of $C_5O_5^{2-}$ in the framework to generate the strong adsorbate−adsorbent interaction. Similar water sorption isotherms can also be found from other Cu(II) 2D or 3D MOFs, e.g., $[Cu_3((TTPB)_2(H_2O)_6)\cdot 5DMF$[60] ($H_2TTPB$ =

https://doi.org/10.1021/acsomega.4c06176
ACS Omega 2024, 9, 40920−40931

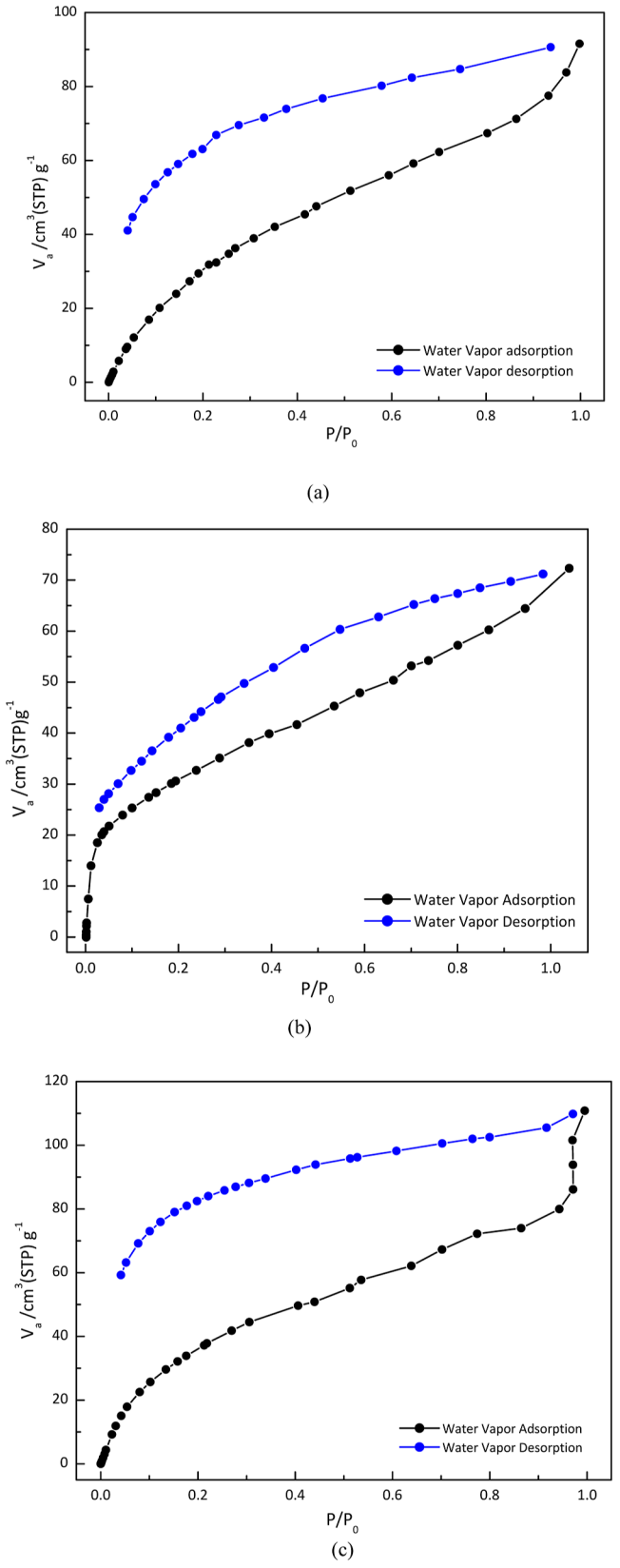

Figure 4. Water vapor adsorption/desorption isotherms of (a) dehydrated **1**, (b) dehydrated **2**, and (c) dehydrated **3**.

1,3,5-tri((4-2*H*-tetrazol-5-yl)phenoxy)benzene) and $[Cu_2(3,4\text{-pyrdc})_2(bpp)_2(H_2O)_4]\cdot 5H_2O$[61] (3,4-pyrdc = 3,4-pyridinedicarboxylate; bpp = 1,3-bis(4-pyridyl)-propane). The hysteretic adsorption behavior to water vapor and the water uptake quantities of **1** and **3** are in comparable with those of other Cu(II) MOFs.[60,61]

The water sorption isotherms of **1** and **3** both exhibit S and type-II isotherm shape, and the hysteresis and retention of water molecules even at low pressure at the end of desorption of **1** and **3** signify a strong interaction of water molecules with the unsaturated Cu(II) sites on the pore surface for **1** and accessible hydrogen-bonded interaction sites from the O atoms of $C_5O_5^{2-}$ ligands to generate the strong adsorbate−adsorbent interaction for **1** and **3**, which are consistent with the structural characterization of **1** and **3**. The water sorption isotherm of **2** is no longer S-shaped but rather exhibits a type I isotherm shape, which is not favorable for the application of atmospheric water harvesting.

CONCLUSIONS

In this work, three Cu(II)-dpds-$C_5O_5^{2-}$ supramolecular architectures, $[Cu_2(dpds)_2(C_5O_5)_2(H_2O)_4]\cdot 3H_2O$ (**1**), $[Cu(dpds)(C_5O_5)]\cdot 3H_2O$ (**2**), and $[Cu_2(dpds)_2(C_5O_5)_2]\cdot 9H_2O\cdot$EtOH (**3**), have been successfully synthesized, and especially, their yields can be controlled by adjusting the contents of EtOH/H_2O (v/v) solvent ratios during the synthesis. It is worth noting that the influencing factors for self-assembly of compounds **1**−**3**, exhibiting 1D to 3D structures with different topologies, are attributed to the coordination spheres of Cu(II) centers with dpds ligands and coordination modes of $C_5O_5^{2-}$ ligands. In **1**, a 1D zigzag chain structure is constructed via cis-coordination sphere of Cu(II) centers with bridging dpds ligands, and the coordination mode of $C_5O_5^{2-}$ is an asymmetrical bidentate chelate (Scheme 1b). In **2**, a 2D layered MOF is built up via trans-coordination sphere of Cu(II) centers with bridging dpds and $C_5O_5^{2-}$ with an asymmetrical μ-1,2,3-bis-bidentate (Scheme 1(i)) to generate 1D rectangle-grid-like open channels. In **3**, a 3D MOF is assembled via both cis- and trans-coordination sphere of Cu(II) centers with bridging dpds ligands and $C_5O_5^{2-}$ with an asymmetrical μ-1,2,3,4-bis-bidentate (Scheme 1(h)). Compounds **1**−**3** show moderate thermal stability evidenced by TGA and PXRD measurements, which is mainly attributed to their stable extended 3D supramolecular architectures by noncovalent interactions, such as intermolecular O−H···O hydrogen bonding and/or $\pi-\pi$ stacking interactions and van der Waals forces. Moreover, the water adsorption profiles show both S and type-II isotherms for **1** and **3**, which are attributed to their structural transformation on the basis of very strong coordination affinity of water molecules with unsaturated Cu(II) sites for **1** and hydrogen-bonding affinity of water molecules with free oxygen atoms of $C_5O_5^{2-}$ in the frameworks to generate the strong adsorbate−adsorbent interactions for **3**.[61−63]

ASSOCIATED CONTENT

Supporting Information

The Supporting Information is available free of charge at https://pubs.acs.org/doi/10.1021/acsomega.4c06176.

Crystal data and structure refinements for **1**, **2**, and **3** at 150 K and **3** at 295 K; selected bond lengths (Å) and angle (deg) for **1**−**3**; O−H···N and O−H···O hydrogen bonds for **1**−**3**; cell parameters of **1**, **2**, and **3** at 150 K and **3**′ at 295 K from single-crystal X-ray diffraction data and **1**′, **2**′, and **3**′ at 423 K from PXRD data; TG

https://doi.org/10.1021/acsomega.4c06176
ACS Omega 2024, 9, 40920−40931

measurements of **1**−**3**; temperature-dependent PXRD patterns and the Le Bail refinement at high temperatures of **1**−**3**; N_2 adsorption/desorption isotherms and CO_2 adsorption of dehydrated species **1**−**3**; and IR spectra of **1**−**3** at room temperature and high temperature (PDF)

Crystallographic data for $[Cu_2(dpds)_2(C_5O_5)_2(H_2O)_4]\cdot 3H_2O$ (**1**) (CIF)

Crystallographic data for $[Cu(dpds)(C_5O_5)]\cdot 3H_2O$ (**2**) (CIF)

Crystallographic data for $[Cu_2(dpds)_2(C_5O_5)_2]\cdot 9H_2O\cdot$ EtOH (**3**) (CIF)

Crystallographic data for compound **4** (CIF)

Accession Codes

Accession codes CCDC2246199, CCDC2246200, CCDC2246201, and CCDC2246202 for **1**, **2**, and **3** at 150 K and **3** at 295 K, respectively, contain the supplementary crystallographic data for this paper.

AUTHOR INFORMATION

Corresponding Authors

Chih-Chieh Wang − *Department of Chemistry, Soochow University, 11102 Taipei, Taiwan;* orcid.org/0000-0001-7286-5597; Phone: 886-2-28819471 ext 6828; Email: ccwang@scu.edu.tw

Yu-Chun Chuang − *National Synchrotron Radiation Research Center, 30076 Hsinchu, Taiwan;* orcid.org/0000-0002-2879-5381; Email: chuang.yc@nsrrc.org.tw

Authors

Pei-Juan Liao − *Department of Chemistry, Soochow University, 11102 Taipei, Taiwan*

Yu-Chen Chung − *Department of Chemistry, Soochow University, 11102 Taipei, Taiwan*

Chi-Yang Shin − *Department of Chemistry, Soochow University, 11102 Taipei, Taiwan*

Yi-Chen Wu − *Department of Chemistry, Soochow University, 11102 Taipei, Taiwan*

Gene-Hsiang Lee − *Instrumentation Center, National Taiwan University, 10617 Taipei, Taiwan*

Su-Ying Chien − *Instrumentation Center, National Taiwan University, 10617 Taipei, Taiwan*

Bo-Hao Chen − *National Synchrotron Radiation Research Center, 30076 Hsinchu, Taiwan;* orcid.org/0000-0002-4127-8338

Complete contact information is available at: https://pubs.acs.org/10.1021/acsomega.4c06176

Author Contributions

Prof. Chih-Chieh Wang conceived and designed the experiments; Miss Pei-Juan Liao, Mr. Chi-Yang Shin, Miss Yi-Chen Wu, and Miss Yu-Chen Chung execute the synthesis experiments, figures drawing, and tables preparation for structural characterization, IR, and TGA measurements; Dr. Gene-Hsiang Lee and Dr. Su-Ying Chien contributed to the data collection, refinement, and structural analysis by single-crystal X-ray diffractometer; Dr. Yu-Chun Chuang and Mr. Bo-Hao Chen contributed to the PXRD experiments by synchrotron radiation light source; and Prof. Chih-Chieh Wang and Dr. Yu-Chun Chuang wrote the paper.

Notes

The authors declare no competing financial interest.

ACKNOWLEDGMENTS

We are grateful to the National Council of Science and Technology (MOST 111-2113-M-031-006) and Soochow University, Taiwan, for financial support.

REFERENCES

(1) Batten, S. R.; Champness, N. R.; Chen, X. M.; Garcia-Martinez, J.; Kitagawa, S.; Öhrström, L.; O'Keeffe, M.; Paik Suh, M.; Reedijk, J. Terminology of Metal-Organic Frameworks and Coordination Polymers (IUPAC Recommendations 2013). *Pure Appl. Chem.* **2013**, *85* (8), 1715−1724.

(2) Batten, S. R.; Champness, N. R.; Chen, X. M.; Garcia-Martinez, J.; Kitagawa, S.; Öhrström, L.; O'Keeffe, M.; Suh, M. P.; Reedijk, J. Coordination polymers, metal−organic frameworks and the need for terminology guidelines. *CrystEngComm* **2012**, *14* (9), 3001−3004.

(3) Li, B.; Chrzanowski, M.; Zhang, Y.; Ma, S. Applications of metal-organic frameworks featuring multi-functional sites. *Coord. Chem. Rev.* **2016**, *307*, 106−129.

(4) Zhang, X.; Wang, W.; Hu, Z.; Wang, G.; Uvdal, K. Coordination Polymers for Energy Transfer: Preparations, Properties, Sensing Applications, and Perspectives. *Coord. Chem. Rev.* **2015**, *284*, 206−235.

(5) Bradshaw, D.; Claridge, J. B.; Cussen, E. J.; Prior, T. J.; Rosseinsky, M. J. Design, Chirality, and Flexibility in Nanoporous Molecule-Based Materials. *Acc. Chem. Res.* **2005**, *38*, 273−282.

(6) Silva, P.; Vilela, S. M. F.; Tome, J. P. C.; Almeida Paz, F. A. Multifunctional Metal−Organic Frameworks: From Academia to Industrial Applications. *Chem. Soc. Rev.* **2015**, *44*, 6774−6803.

(7) Li, S.; Huo, F. Metal−Organic Framework Composites: From Fundamentals to Applications. *Nanoscale* **2015**, *7*, 7482−7501.

(8) Janiak, C.; Vieth, J. K. MOFs, MILs and more: concepts, properties and applications for porous coordination networks (PCNs). *New J. Chem.* **2010**, *34*, 2366−2388.

(9) He, Y.; Li, B.; O'Keeffe, M.; Chen, B. Multifunctional metal−organic frameworks constructed from meta-benzenedicarboxylate units. *Chem. Soc. Rev.* **2014**, *43* (16), 5618−5656.

(10) Lin, Z. J.; Lu, J.; Hong, M.; Cao, R. Metal−organic frameworks based on flexible ligands (FL-MOFs): structures and applications. *Chem. Soc. Rev.* **2014**, *43* (16), 5867−5895.

(11) Lu, W.; Wei, Z.; Gu, Z.-Y.; Liu, T.-F.; Park, J.; Park, J.; Tian, J.; Zhang, M.; Zhang, Q.; Gentle III, T.; Bosch, M.; et al. Tuning the structure and function of metal-organic frameworks via linker design. *Chem. Soc. Rev.* **2014**, *43*, 5561−5593.

(12) Zhou, H.-C.; Kitagawa, S. Metal−Organic Frameworks (MOFs). *Chem. Soc. Rev.* **2014**, *43*, 5415−5418.

(13) He, Y.; Zhou, W.; Qian, G.; Chen, B. Methane storage in metal−organic frameworks. *Chem. Soc. Rev.* **2014**, *43*, 5657−5678.

(14) Karmakar, A.; Paul, A.; Mahmudov, K. T.; Guedes da Silva, M. F. C.; Pombeiro, A. J. L. pH dependent synthesis of Zn(ii) and Cd(ii) coordination polymers with dicarboxyl-functionalized arylhydrazone of barbituric acid: photoluminescence properties and catalysts for Knoevenagel condensation. *New J. Chem.* **2016**, *40*, 1535−1546.

(15) Paul, A.; Karmakar, A.; Guedes da Silva, M. F. C.; Pombeiro, A. J. L. Amide functionalized metal−organic frameworks for diastereoselective nitroaldol (Henry) reaction in aqueous medium. *RSC Adv.* **2015**, *5*, 87400−87410.

(16) Karmakar, A.; Oliver, C. L.; Roy, S.; Öhrström, L. The synthesis, structure, topology and catalytic application of a novel cubane-based copper(ii) metal−organic framework derived from a flexible amido tripodal acid. *Dalton Trans.* **2015**, *44*, 10156−10165.

(17) Steel, P. J. Aromatic nitrogen heterocycles as bridging ligands; a survey. *Chem. Rev.* **1990**, *106*, 227−265.

(18) Bon, V.; Senkovska, I.; Weiss, M. S.; Kaskel, S. Tailoring of network dimensionality and porosity adjustment in Zr- and Hf-based MOFs. *CrystEngComm* **2013**, *15*, 9572−9577.

(19) Fukushima, T.; Horike, S.; Inubushi, Y.; Nakagawa, K.; Kubota, Y.; Takata, M.; Kitagawa, S. Solid Solutions of Soft Porous

https://doi.org/10.1021/acsomega.4c06176
ACS Omega 2024, 9, 40920−40931

Coordination Polymers: Fine-Tuning of Gas Adsorption Properties. *Angew. Chem., Int. Ed.* **2010**, *49*, 4820−4824.
(20) Zhou, X.; Lu, H.; Zhao, F.; Yu, G. Atmospheric Water Harvesting: A Review of Material and Structural Designs. *ACS Mater. Lett.* **2020**, *2*, 671−684.
(21) Wang, C. C.; Ke, S. Y.; Chen, K. T.; Sun, N. K.; Liu, W. F.; Ho, M. L.; Lu, B. J.; Hsieh, Y. T.; Chuang, Y. C.; Lee, G. H.; Huang, S. Y.; et al. Sponge-Like Water De-/Ad-Sorption versus Solid-State Structural Transformation and Colour-Changing Behavior of an Entangled 3D Composite Supramolecuar Architecture, $[Ni_4(dpe)_4(btc)_2(Hbtc)(H_2O)_9]\cdot 3H_2O$. *Polymers* **2018**, *10*, 1014.
(22) Ke, S. Y.; Chang, Y. F.; Wang, H. Y.; Yang, C. C.; Ni, C. W.; Lin, G. Y.; Chen, T. T.; Ho, M. L.; Lee, G. H.; Chuang, Y. C.; Wang, C. C. Self-Assembly of Four Coordination Polymers in Three-Dimensional Entangled Architecture Showing Reversible Dynamic Solid-State Structural Transformation and Color-Changing Behavior upon Thermal Dehydration and Rehydration. *Cryst. Growth Des.* **2014**, *14* (8), 4011−4018.
(23) Wang, C. C.; Tsai, J. H.; Ke, S. Y.; Lee, G. H.; Chuang, Y. C.; Yang, E. C. Structural Characterization, Water Adsorption, and Magnetic Properties of Two Composite Mn(II)−Squarate−dpe Supramolecular Architectures. *Cryst. Growth Des.* **2020**, *20* (8), 5395−5405.
(24) Haiduc, I. Inverse coordination chemistry: oxocarbons, other polyoxo carbocyclic molecules and oxygen heterocycles as coordination centers. Topology and systematization. *J. Coord. Chem.* **2020**, *73*, 2117−2170.
(25) Mautner, F. A.; Fischer, R. C.; Torvisco, A.; Grant, E. P.; Romain, D. S. S.; Salem, N. M. H.; Louka, F. R.; Massoud, S. S. Copper(II) and zinc(II) complexes bridged by benzenoid aromatic oxocarbon and dicarboxylate dianions. *Polyhedron* **2023**, *234*, 116327.
(26) Massoud, S. S.; Williams, G. F.; Louka, F. R.; Henary, M. M.; Herchel, R.; Trávníček, Z.; Fischer, R. C.; Mautner, F. A. Croconato-bridged copper(ii) complexes: synthesis, structure and magnetic characterization. *New J. Chem.* **2017**, *41*, 3846−3856.
(27) Massoud, S. S.; Vicente, R.; Fontenot, P. R.; Gallo, A. A.; Mikuriya, M.; Albering, J. H.; Mautner, F. A. Polynuclear croconato-bridged-copper(II) complexes derived from tri- and tetra-dentate amines. *Polyhedron* **2012**, *46*, 66−73.
(28) Carranza, J.; Sletten, J.; Brennan, C.; Lloret, F.; Cano, J.; Julve, M. Mono-di- and trinuclear 2,3,5,6-tetrakis(2-pyridyl)pyrazine (tppz)-containing copper(ii) complexes: syntheses, crystal structures and magnetic properties. *Dalton Trans.* **2004**, *23*, 3997−4005.
(29) Wang, C. C.; Yang, C. H.; Lee, G. H. Synthesis and Structural Characterization of $[Na_2M(C_5O_5)_2(H_2O)_2]\cdot 4H_2O$ (M = Ni^{II}, Cu^{II}). *Inorg. Chem.* **2002**, *41*, 1015−1018.
(30) Castro, I.; Sletten, J.; Glærum, L. K.; Lloret, F.; Faus, J.; Julve, M. Syntheses crystal structures and electronic properties of $[Cu(bipym)(C_5O_5)(H_2O_2)]\cdot H_2O$ and $[Cu_2(bipym)(C_5O_5)_2(H_2O)_2\cdot 4H_2O$ (bipym = 2,2′-bipyrimidine). *J. Chem. Soc., Dalton Trans.* **1994**, 2777−2782.
(31) Castro, I.; Sletten, J.; Faus, J.; Julve, M. Complex formation between croconate ($C_5O_5^{2-}$) and $Cu^{II}L$ [L = 2,2′-bipyridine (bipy), 2,2′:6′,2″-terpyridine or bis(2-pyridylcarbonyl)amide anion] in dimethyl sulfoxide solution. Crystal structure of $[Cu(bipy)(C_5O_5)(H_2O)]$. *J. Chem. Soc., Dalton Trans.* **1992**, 2271−2275.
(32) Castro, I.; Calatayud, M. L.; Lloret, F.; Sletten, J.; Julve, M. Syntheses crystal structures and magnetic properties of di- and trinuclear croconato-bridged copper(ii) complexes. *J. Chem. Soc., Dalton Trans.* **2002**, 2397−2403.
(33) Castro, I.; Calatayud, M. L.; Sletten, J.; Julve, M.; Lloret, F. Squarate et croconate pour le design de complexes mono- et bidimensionnels de Cu(II) à pont oxamidato : synthèse, structures cristallines et propriétés magnétiques de [Cu2(apox)(C4O4)(H2O)-2]n·n H2O and [Cu4(apox)2(C5O5)2]·6 H2O. *Acad. Sci., Ser. IIc: Chim.* **2001**, *4*, 235−243.
(34) Castro, I.; Sletten, J.; Faus, J.; Julve, M.; Journaux, Y.; Lloret, F.; Alvarez, S. Exchange interaction through a croconato bridge: synthesis, crystal structure, and magnetic properties of (.mu.-croconato)bis[{bis(2-pyridylcarbonyl)amido}copper(II)] trihydrate. *Inorg. Chem.* **1992**, *31* (10), 1889−1894.
(35) Broucacabarrecq, C.; Trombe, J. C. f element croconates 1. Lanthanide croconates — synthesis, crystal structure and thermal behaviour. *Inorg. Chim. Acta* **1992**, *191*, 227−240.
(36) Artizzu, F.; Deplano, P.; Pilia, L.; Serpe, A.; Marchio, L.; Bernot, K.; Mercuri, M. L. Croconato-containing M(III) (M = Ga, Er) complexes as potential building blocks for mono/multifunctional molecular materials. *Inorg. Chim. Acta* **2011**, *370*, 474−481.
(37) de Paula, E. E. B.; Visentin, L. C.; Yoshida, M. I.; de Oliveira, L. F. C.; Machado, F. C. Unprecedented μ-1,2-bis(monodentate) coordination mode of croconate dianion (C5O52−): Synthesis and crystal structures of manganese- and copper-based coordination polymers. *Polyhedron* **2011**, *30*, 213−220.
(38) Wang, C. C.; Ke, M. J.; Tsai, C. H.; Chen, I. H.; Lin, S. I.; Lin, T. Y.; Wu, L. M.; Lee, G. H.; Sheu, H. S.; Fedorov, V. E. $[M(C_5O_5)_2(H_2O)n]^{2-}$ as a Building Block for Hetero- and Homo-bimetallic Coordination Polymers: From 1D Chains to 3D Supramolecular Architectures. *Cryst. Growth Des.* **2009**, *9*, 1013−1019.
(39) Vicente, R.; Cano, J.; Ruiz, E.; Massoud, S. S.; Mautner, F. A. Squarato−Metal(II) Complexes. 2. Unusual Bonding Mode for a Squarato-Bridged Trinuclear Copper(II) Complex. *Inorg. Chem.* **2008**, *47*, 4648−4655.
(40) Wang, C. C.; Dai, S. C.; Lin, H. W.; Lee, G. H.; Sheu, H. S.; Lin, Y. H.; Tsai, H. L. Assembly of Metal Coordination Framework, $[M^{II}(C_5O_5)(dpe)]$, with a 2D Bi-layer Architecture: Thermal Stability and Magnetic Properties (M = Mn, Fe, Cd and Co; dpe = 1,2-bis(4-pyridyl)ethane). *Inorg. Chim. Acta* **2007**, *360*, 4058−4067.
(41) Maji, T. K.; Konar, S.; Mostafa, G.; Zangrando, E.; Lu, T. H.; Ray Chaudhuri, N. Self-assembly of new three-dimensional molecular architectures of Cd(II) and Ag(I)−Na(I) using croconate as a building block. *J. Chem. Soc., Dalton Trans.* **2003**, 171−175.
(42) Maji, T. K.; Ghoshal, D.; Zangrando, E.; Ribas, J.; Chaudhuri, N. R. A novel 2D mixed valence copper(I/II) rectangular grid constructed with pyrazine and croconate. *CrystEngComm* **2004**, *6*, 623−626.
(43) Wang, C. C.; Kuo, C. T.; Yang, J. C.; Lee, G. H.; Shih, W. J.; Sheu, H. S. Assemblies of Two New Metal−Organic Frameworks Constructed from Cd(II) with 2,2′-Bipyrimidine and Cyclic Oxocarbon Dianions $CnOn^{2-}$ (n = 4, 5). *Cryst. Growth Des.* **2007**, *7*, 1476−1482.
(44) Wang, C. C.; Tseng, S. M.; Lin, S. Y.; Liu, F. C.; Dai, S. C.; Lee, G. H.; Shih, W. J.; Sheu, H. S. Assemblies of Two Mixed-ligands Coordination Polymers with 2-D MOFs Constructed from M(II) ions with Croconate ($C_5O_5^{2-}$) and 1,2-bis-(4-pyridyl)ethylene (bpe) (M = Cd and Zn). *Cryst. Growth Des.* **2007**, *7*, 1783−1790.
(45) Louka, F. R.; Stewart, A. D.; Regel, E.; Mautner, F. A.; Demeshko, S.; Meyer, F.; Massoud, S. S. Squarato-metal(II) complexes: Part 5. Polynuclear copper(II) complexes bridged by squarate and croconate dianions. *Inorg. Chem. Commun.* **2012**, *22*, 60−64.
(46) Manna, S. C.; Ghosh, A. K.; Zangrando, E.; Chaudhuri, N. R. 3D supramolecular networks of Co(II)/Fe(II) using the croconate dianion and a bipyridyl spacer: Synthesis, crystal structure and thermal study. *Polyhedron* **2007**, *26*, 1105−1112.
(47) Wang, C. C.; Yang, C. H.; Tseng, S. M.; Lee, G. H.; Chiang, Y. P.; Sheu, H. S. Self-Assembly of a Mixed-Ligand Metal-Coordination Polymeric Network of Cadmium(II) Croconate with 4,4′-Bipyridine. *Inorg. Chem.* **2003**, *42*, 8294−8299.
(48) Wang, C. C.; Lin, H. W.; Yang, C. H.; Liao, C. H.; Lan, I. T.; Lee, G. H. Synthesis and Structure of A Novel Two-dimensional Bi-layer Framework of $[M(C_5O_5)(dpe)]$ Coordination Polymer. *New J. Chem.* **2004**, *28*, 180−182.
(49) Wang, C. C.; Liu, F. C.; Chiu, C. K.; Song, Y.; Wang, S. C.; Wang, Y.; Lee, G. H.; Sheu, H. S.; Yang, E. C. Synthesis, Structural Characterization and Magnetic Behavior of a 2D Bi-Layer MOF, $\{[Ni_2(C_5O_5)_2(bpe)_2]\cdot H_2O\}_n$ (bpe = 1,2-bis(4-pyridyl)ethylene). *CrystEngComm* **2011**, *13*, 118−123.

https://doi.org/10.1021/acsomega.4c06176
ACS Omega 2024, 9, 40920−40931

(50) Hopf, H.; Sherburn, M. S. Chapter 5: Oxocarbons, Pseudo-oxocarbons and Squaraines. In *Cross Conjugation: Modern Dendralene, Radialene and Fulvalene Chemistry*; de Oliveira, V. E., Diniz, R., Machado, F. C., de Oliveira, L. F. C., Eds.; Wiley, 2016; .
(51) *SAINT V8.40B*; Bruker AXS GmbH: Karlsruhe, Germany, 2019.
(52) Krause, L.; Herbst-Irmer, R.; Sheldrick, G. M.; Stalke, D. Comparison of silver and molybdenum microfocus X-ray sources for single-crystal structure determination. *J. Appl. Crystallogr.* **2015**, *48*, 3−10.
(53) Sheldrick, G. M. Crystal structure refinement with SHELXL. *Struct. Chem.* **2015**, *71*, 3−8.
(54) *APEX4 v.2021.10.10−0*; Bruker AXS GmbH: Karlsruhe, Germany, 2021.
(55) Toby, B. H.; Von Dreele, R. B. GSAS-II: the genesis of a modern open-source all-purpose crystallography software package. *J. Appl. Crystallogr.* **2013**, *46*, 544−549.
(56) O'Donnell, J. H.; Von Dreele, R. B.; Chan, M. K. Y.; Toby, B. H. A scripting interface for GSAS-II. *J. Appl. Crystallogr.* **2018**, *51*, 1244−1250.
(57) Ito, M.; Weiss, R. New Aromatic Anions. IV. Vibrational Spectra and Force Constants for $C_4O_4^{-2}$ and $C_5O_5^{-2}$. *J. Am. Chem. Soc.* **1963**, *85*, 2580−2584.
(58) Sing, K. S. W. Reporting physisorption data for gas/solid systems with special reference to the determination of surface area and porosity (Recommendations 1984). *Pure Appl. Chem.* **1985**, *57*, 603−619.
(59) Thommes, M.; Kaneko, K.; Neimark, A. V.; Olivier, J. P.; Rodriguez-Reinoso, F.; Rouquerol, J.; Sing, K. S. Physisorption of gases, with special reference to the evaluation of surface area and pore size distribution (IUPAC Technical Report). *Pure Appl. Chem.* **2015**, *87*, 1051−1069.
(60) He, H.; Song, Y.; Sun, F.; Zhao, N.; Zhu, G. Sorption Properties and Nitroaromatic Explosives Sensing Based on Two Isostructural Metal−Organic Frameworks. *Cryst. Growth Des.* **2015**, *15*, 2033−2038.
(61) Halder, A.; Bhattacharya, B.; Dey, R.; Maity, D. K.; Ghoshal, D. Reversible Phase Transformation in Three Dynamic Mixed-Ligand Metal−Organic Frameworks: Synthesis, Structure, and Sorption Study. *Cryst. Growth Des.* **2016**, *16*, 4783−4792.
(62) Rieth, A. J.; Yang, S.; Wang, E. N.; Dincă, M. Record Atmospheric Fresh Water Capture and Heat Transfer with a Material Operating at the Water Uptake Reversibility Limit. *ACS Cent. Sci.* **2017**, *3*, 668−672.
(63) Canivet, J.; Bonnefoy, J.; Daniel, C.; Legrand, A.; Coasne, B.; Farrusseng, D. Structure−property relationships of water adsorption in metal−organic frameworks. *New J. Chem.* **2014**, *38*, 3102−3111.

https://doi.org/10.1021/acsomega.4c06176
ACS Omega 2024, 9, 40920−40931